International Journal of Heat and Mass Transfer 54 (2011) 118–125

Contents lists available at ScienceDirect

International Journal of Heat and Mass Transfer

journal homepage: www.elsevier.com/locate/ijhmt

Optimization of microscale vortex generators in a microchannel using advanced response surface method

Beom Seok Kim, Bong Seop Kwak, Sangwoo Shin, Sanghoon Lee, Kyung Min Kim, Hyo-Il Jung, Hyung Hee Cho *

Department of Mechanical Engineering, Yonsei University, 262, Seongsanno, Seodaemun-gu, Seoul 120-749, Republic of Korea

ARTICLE INFO

Article history:
Received 25 July 2010
Received in revised form 8 September 2010
Accepted 8 September 2010
Available online 27 October 2010

Keywords:
Rib turbulator
Micromixer
Mass transport
Optimization
Response surface method

ABSTRACT

Mixing based on mass diffusion and advective flow at low Reynolds number is important on design of microscale vortex generators. We studied on the optimization of micromixer for the improvement of mass transport using an advanced response surface method to be closely approximate the real map of mixing performance. We considered four rib geometries simultaneously; rib angle, rib height, rib width, and rib spacing. The optimized microchannel was occurred at a micromixer configuration where θ, d/h, a/d, and b/d were 35.6°, 0.7, 0.127, and 1.10, respectively. The channel length to obtain the mixing uniformity over 95% was 1344 μm.

1. Introduction

Mixing based on mass diffusion and induced advective flow is very important on design of micromixer in microfluidic devices. The purpose of a mixing in microfluidics is to reduce the lengthscale required to obtain adequate mixing performance with uniform concentration for the compact microfluidic devices [1–3]. Generally in microscale channel, liquid streams have low Reynolds number, so the mixing between difference species is readily dependent on mass diffusion. Therefore, vortex generators are required to enhance the mixing performance because the mixing by only mass diffusion is exceedingly slow. A passive micromixer as a vortex generator generates vortex streams and advective flow motions in microchannel and thus enhances the mixing performance by increasing the interfacial mixing areas between species.

Vortex generators can be used in various research fields such as macro-to-microscale heat transfer for the improvement of cooling performance and flow control [3–8] as well as biology, biomedicine and lab-on-a-chip applications such as DNA analysis, cell separation and drug delivery systems [9–11]. Especially for miniaturized devices on which the different chemicals or species are mixed, such as micro calorimeters and microfluidic thermal sensors, when the area or lengthscale of interest (i.e., sensing part) is large, it can cause instability and reduce sensitivity of output signal from the sensors which detect the local-area averaged signal. It is because that the large area or lengthscale can be affected by spatial and temporal fluctuation of non-uniform fluidic/thermal characteristics and also attenuate the signal due to the gradient of them [12,13]. Therefore, it is required to maximize the efficiency of mass transport by minimizing the duration of mixing and shrink the lengthscale of fluidic channel in lab-on-a chip devices to obtain high sensitivity and reliability.

Many studies have focused on not only the design of the channel structure like serpentine laminating structure and curved channel for Dean vortex generation [14,15], but the mixer structure, including the staggered herringbone [1], slanted groove [16,17], and barrier embedded with slanted groove [18] and combinatorial one [19]. For the slanted groove mixers, it has been known that several design parameters affect the mixing performance [16,20,21]. Especially, Lynn and Dandy optimized grooved mixers with respect to channel aspect ratio, groove depth ratio, and ridge length [22]. However, in some previous studies including previous one, they fixed the value of slanted rib angle at 45° [1,22], even though the slanted rib angle is the most significant factor in vortex formation as reported by Kim et al. [23].

For the performance optimization, numerical evaluation of mixing characteristics is required according to the variation of design variables. Many papers have recently been published on fluid characteristics in concentration distribution, velocity field or secondary flow intensity in a local region based on computational fluid dynamics (CFD) using commercial code such as Fluent [22,24], CFD-ACE+ [14,25] and CFX [7,17]. In particular, Stroock et al. [16] and Schonfeld [17] compared analytical and numerical results with experimental ones for generating helical flow with a mixer in a microfluidic channel, and found reasonable agreement for both approaches.

* Corresponding author. Tel.: +82 2 2123 2828; fax: +82 2 312 2159.
E-mail address: hhcho@yonsei.ac.kr (H.H. Cho).

0017-9310/$ - see front matter © 2010 Elsevier Ltd. All rights reserved.
doi:10.1016/j.ijheatmasstransfer.2010.09.061

In addition to the researches of novel configuration design, it is necessary to evaluate the mixing performance quantitatively and suggest the optimal design guidelines on micromixer based on optimization technique. To date, for practical application of micromixer there are few studies that present design guidelines for the optimization to maximize the mixing performance by increasing mass transport and minimize the lengthscale of the required channel. Therefore it is exceedingly of use to make design correlations with structural design variables using an optimization technique. Using optimization technique such as response surface method, we can evaluate the design variables on the mixing characteristics and suggest the most effective configurations with high reliability of optimization to obtain uniform mixture concentration and high sensitivity of microfluidic sensing devices.

In this paper, we intended to optimize the mixing performance by controlling design variables of micromixer using an advanced response surface method (α-RSM). Here, we considered four design variables simultaneously: slanted rib angle as well as rib height, rib width, rib spacing. The effect of design variables were discussed through detailed analyses procedures of liquid mixing behavior. We evaluated the optimal design point and correlated design variables as a design guideline for the minimal lengthscale of microchannel.

2. Materials and methods

2.1. Modeling and design variables

Fig. 1 shows the geometry of the channel used in this study [13,26]. We considered four design variables simultaneously; these are the slanted rib angle, the rib height, the rib width, and the rib spacing. These variables, except for the rib slanted angle, were converted into three nondimensional combinations of variables: the ratio of rib height to channel height d/h, the ratio of rib width to rib height a/d, and the ratio of rib spacing to rib height b/d. The ranges of the design variables are limited like shown in Table 1 by considering the practical bio-agents with a size of from five to tens of micron. Thirty rib-shaped mixers with an angle θ were installed in a T-shaped microchannel with a fixed aspect ratio of one and a square cross-section of 100×100 μm.

2.2. Fabrication process of microchannel with mixers

Fig. 2 shows the fabrication process of microchannel with micromixers. We fabricate micromixer using silicon deep reactive ion etching processes as shown in Fig. 2. To prepare the device, two photomasks are used: one to make upper polydimethylsiloxane (PDMS) layer, and the other to make lower PDMS layer.

Table 1
Design variables and ranges in RSM processes.

Variables		Lower bound	Upper bound
x_1	θ	15	60
x_2	d/h	0.2	0.7
x_3	a/d	0.05	4
x_4	b/d	1	15

First, AZ5214 (Clariant Industries Ltd.) image reverse photosensitive polymer layer was double spin coated at 2500 rpm on a silicon wafer. Second, double exposure was performed using 365 nm wavelength UV (Karl Suss MA6 Mask Aligner, 14 mJ/cm^2) for 2.4 and 14 s, respectively, for negative image of photoresist layer. Third, developing process was performed using AZ300 (Clariant Industries Ltd.) developer for 45 s. Fourth, deep silicon trench etching process was performed. After silicon bulk etching process, photoresist was removed by microwave plasma asher and passivation layer (C_4F_8) was deposited. The same procedure was performed for the lower layer. After making silicon molding, the standard PDMS fabrication process was performed for making the upper and the lower channel layer. At last, two layers were irreversibly bonded using oxygen plasma with alignment.

2.3. Visualization of liquid mixing

The fluorescein isothiocyanate (FITC, Sigma Aldrich) was used for visualizing mixing behavior in the micromixer. The FITC was diluted using deionized water at 100 mM concentration. For the visualization of mixtures, we supplied deionized water through two channel inlets, one of which had a stream of pure deionized water while the other had a stream mixed with fluorescent dye. The flow rate at each inlet of the T-shaped channel were at 10 μL/min, which corresponds to a Reynolds number of 1.69. Reynolds number of 1.69 is very low which results in absolutely laminar flow. The images of the fluorescent dye at the mid-plane of the channel from the bottom and cross-section planes were obtained using a confocal microscope (LSM 510 META, Carl Zeiss).

2.4. Numerical analysis of mixing behavior

2.4.1. Governing equations and numerical method

We used water (H_2O) and methyl alcohol (CH_3OH) as two sample liquids [13,26,27]. Under laminar flow conditions, mass diffusion between the liquid species is dominant for mixing phenomena [28]. Therefore, we considered a mass diffusion equation without any chemical reaction, as well as the incompressible continuity equation and the Navier–Stokes equation [29]:

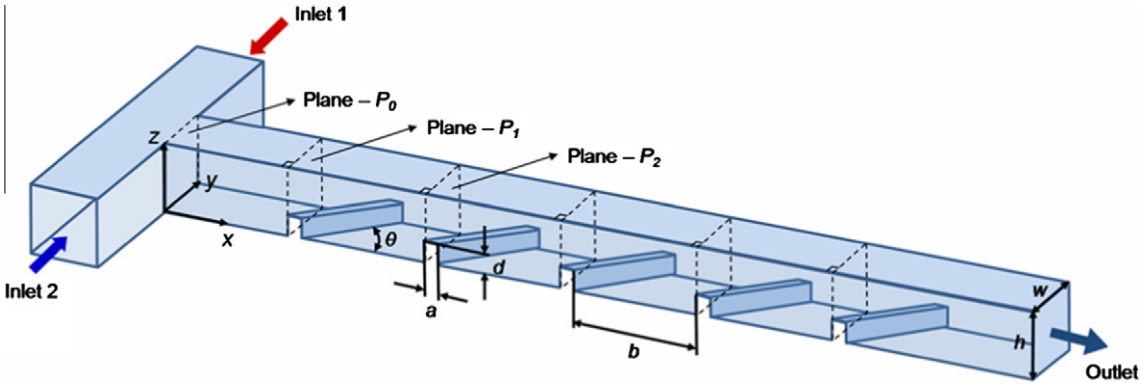

Fig. 1. Schematic of the microchannel with rib-roughened mixers.

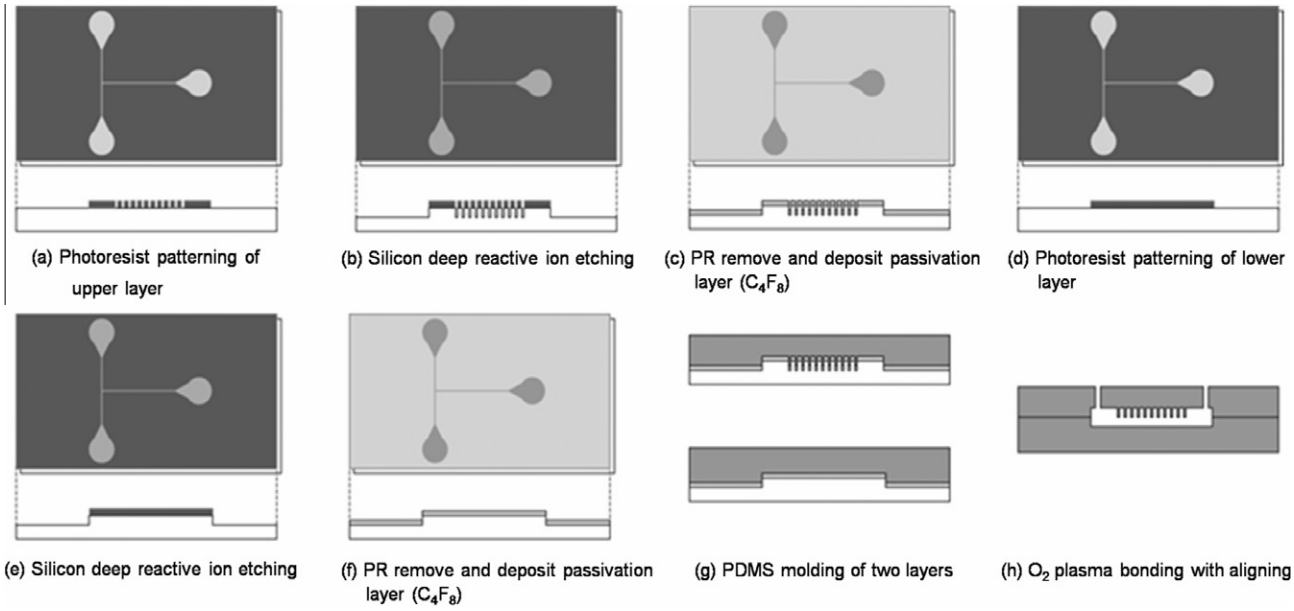

Fig. 2. Fabrication process of microchannel with micromixer.

$$\nabla \cdot \overline{V} = 0 \tag{1}$$

$$\rho \frac{D\overline{V}}{Dt} = -\nabla p + \mu \nabla^2 \overline{V} \tag{2}$$

$$\overline{G} \cdot \nabla m_j - \nabla \cdot \gamma_j \nabla m_j = 0 \tag{3}$$

$$\gamma_j = \rho \overline{D}_j, \quad \overline{D}_j = D_{12} = \cdots = D_{ij} \tag{4}$$

where $\overline{V}$, ρ, p, t, and μ indicate the stream velocity, density, pressure, time and viscosity of fluid, respectively. And $\overline{G}$, m_j, and Dj represent the mass flux (mass flow rate per unit of normal area), mass concentration of component j, and binary mass diffusion coefficient, respectively. Based on the Schmidt number and liquid properties, we used a value of 1.570×10^{-9} m^2/s as the diffusion coefficient between water and methyl alcohol to achieve accurate results for the mass diffusion [30]. The Schmidt number can be calculated by $Sc = \nu/D_{ij} = \mu/\rho D_{ij}$ where ν is the kinematic viscosity.

The number of meshes was 2.4–3.2 millions, which was determined based on grid independence tests. Then numerical analyses were conducted using Fluent 6.3.26 (ANSYS) for steady state and laminar flow conditions with double-precision accuracy. However, when calculating a mass diffusion problem based on a finite volume, the results are highly dependent on the shape and the number of meshes. In the case of an unstructured mesh, it is highly possible that truncation and discretization errors will occur when calculating solutions to the partial differential equations, especially during the diffusion analysis of the fluids [31,32]. These numerical errors can exaggerate the diffusion phenomena between species, resulting in better mixing performance in the flow direction. Therefore, for reliable calculation of the diffusive/convective behavior of liquids, we used only structured hexahedral meshes with a skewness of less than 0.78, calculated the mass diffusion of Eq. (3) using a third-order monotone upstream-centered scheme for conservation laws, and considered the momentum of fluids according to Eqs. (1) and (2) using a second-order upwind scheme.

2.4.2. Evaluation of mixing performance

We used the percentage mixed, $P(\%)$, to quantify the mixing characteristics as expressed by Johnson et al. [27]. $P(\%)$ represents the standard deviation of mass concentration distribution between on each cross-section plane (plane P_i in Fig. 1) and on the first junction plane (plane P_0 in Fig. 1) as a reference one. It can be referred to as the difference between mass concentration on the junction plane (plane P_0 in Fig. 1) when there is no mixing and that on the plane of interest (plane P_i in Fig. 1). The following formula gives the percentage mixed used in this study:

$$P(\%) = \left(1 - \frac{\sqrt{\frac{1}{N}\sum_{i=1}^{N}\left(M_i^{mix} - \overline{M_i^{mix}}\right)^2}}{\sqrt{\frac{1}{N}\sum_{i=1}^{N}\left(M_i^{0} - \overline{M_i^{mix}}\right)^2}} \right) \times 100 \tag{5}$$

where N, M_i^{mix}, M_i^0, and $\overline{M}_i^{mix}$ are the total number of computational node, the concentration of methyl alcohol at computational node i on the plane of interest, the concentration of methyl alcohol at computational node i if no mixing or diffusion occurs on the reference plane, and the averaged concentration of the mixed solution at computational node i on the reference plane, respectively [13].

2.5. Advanced response surface method with functional variables

The standard response surface method (RSM) is an optimization technique that results in an approximation for selecting the design geometries [33,34]. In RSM, it is assumed that the true functional relationship $y = f(x_1, x_2, \ldots, x_k) + \varepsilon$ is unknown. Here $x_1, x_2, \ldots, x_k$ are the design variables and ε is the usual random error component. In this study, we used a second-order approximated model, which is the Taylor series approximation; through second-order terms, these results in a model of the type

$$\begin{aligned} y &= C_0 + C_1 x_1 + \cdots + C_k x_k + C_{11} x_1^2 + \cdots + C_{kk} x_k^2 + C_{12} x_1 x_2 \\ &\quad + \cdots + C_{k-1,k} x_{k-1} x_k + \varepsilon \\ &= C_0 + \sum_{i=1}^{k} C_{ii} x_i^2 + \sum \sum_{i<j=2}^{k} C_{ij} x_i x_j + \varepsilon \end{aligned} \tag{6}$$

Using this form, we can search for the local optimum values within the region of interest [35]. However, the standard RSM has some shortcomings in approximating complex functions, obtaining a low physical response (local sensitivity), and selecting the design variable ranges. Therefore, we used the advanced-RSM technique proposed by Kim et al. [23,36]. The advanced-RSM technique improves the R-square value, R^2, which is the coefficient of determination, of correlation function for the response surface in design space.

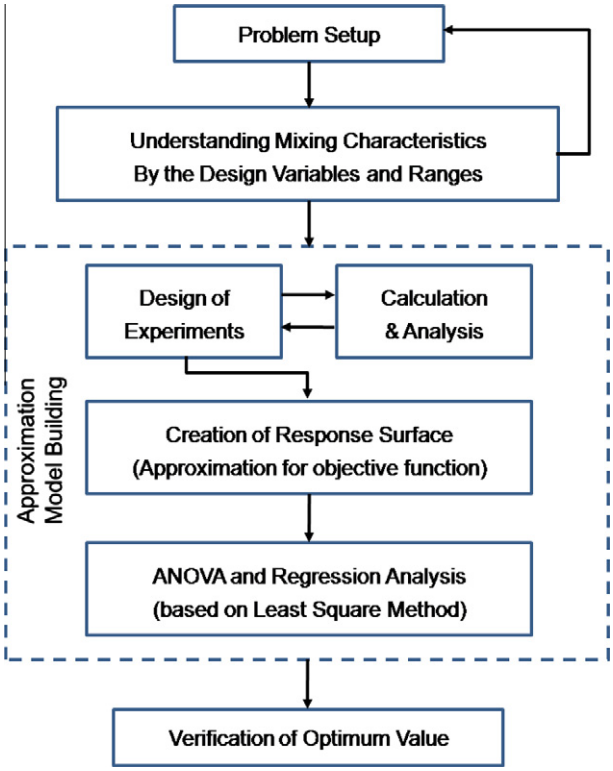

Fig. 3. Flowchart of the advanced response surface method processes.

Because the advanced-RSM approaches to the response value with the equation not described by the original but by the substituted values according to the functional variables, the derived correlation function for the response surface can have more reliable proximity to cover all design points that were used to present the discrete response values. Therefore, the advanced-RSM could have comparatively high R^2 value than the standard RSM. The procedure to find forms of each functional variable includes understanding the characteristics of the design variables in a certain design range and thereby changing the variables x_i into the functional design variables $f(x_i)$ as follows:

$$y = C_0 + \sum_{i=1}^{k} C_i f(x_i) + \sum_{i=1}^{k} C_{ii} f^2(x_i) + \sum \sum_{i<j=2} C_{ij} f(x_i) f(x_j) + \varepsilon \qquad (7)$$

where $f(x_i)$ can be in the form $sin(x_i)$, $log(x_i)$, $exp(x_i)$ and so on according to the relationship between the original variables and the response value. We can determine the exact form of each functional variable by the parametric studies to confirm the effect of each original variable. This advanced RSM has the principal advantage of approximations that are closer to real data than the general non-functional RSM. Overall procedures for the response surface method with functional variables are presented in Fig. 3 with the following steps: (a) select design variables and spaces in design parameters; (b) estimate and determine the correlation characteristics for the variables; (c) construct design points using design of experiments (DOE); (d) evaluate performance using experiments or numerical analysis; (e) generate response surface and analysis of variance (ANOVA); (f) create the approximation equations (obtain the coefficient value, C_i in Eq. (7)); (g) implement optimization processes to find the optimum values; (h) verify the optimum value against the calculation for the optimum design point [23,36].

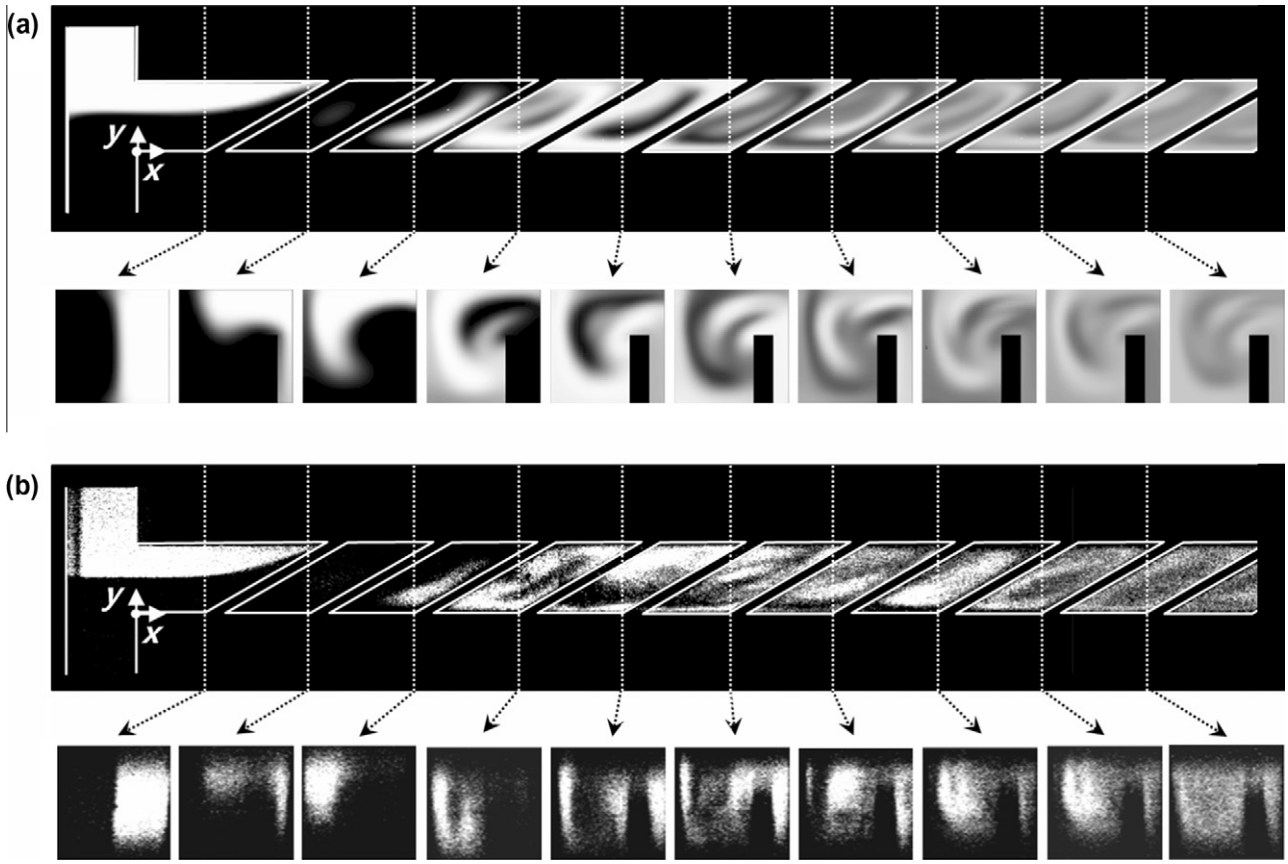

Fig. 4. Qualitative comparisons of mixing characteristics obtained from numerical analysis and experimental visualization.

Based on the evaluation the mixing characteristics by the four design variables, the unknown coefficients in Eq. (7) can be estimated by the least squares method using the functional variables. To achieve a reliable response surface in fluid dynamics and find the global minimum point of the objective function accurately, we calculated and analyzed using 47 design of experimental (DOE) points composed of 25 data points extracted by the D-optimal method, which provides an efficient approach for RSM building as suggested by Mitchell [37] within the design ranges and the others used in the parametric studies that will be mentioned in results section. To assure the optimal point as a global minimum, we conducted the same optimization procedures four times by reducing the design ranges of variables about 20% per each time based on an expected optimal point. The statistics give R^2 value of 0.937.

To determine the optimum values of the design variables using the percentage mixed, we define the objective function $y = f(x_1, x_2, x_3, x_4) = [\Delta L_{95}]_{min}$ where ΔL_{95} is the distance from the junction plane (P_0 in Fig. 1) to the plane of 95% of the P(%) value in the x-axis direction [1]. ΔL_{95} is determined by interpolating the distribution of P(%) on each cross-section along the x-direction from the plane P_0 in Fig. 1 to outlet plane.

3. Results and discussion

3.1. Convective and diffusive behavior of streams

Fig. 4 shows the qualitative results of the contour variation due to mixing obtained by numerical analysis (Fig. 4a) and experimental visualization (Fig. 4b). The mixer had parameter values of $\theta = 30.0°$, $d/h = 0.6$, $a/d = 0.5$, and $b/d = 2$. Fig. 4a and b shows the normalized mass fraction contour of the methyl alcohol resulting from the numerical calculation and the fluorescence image of deionized water obtained by experimental visualization [13] in the mid-plane at $z = 50$ μm from the bottom, respectively. And we also presented the series of mass fraction contours at the cross-section in front of each mixer corresponding to the analysis and the experiment. The configured mixers generate a transverse velocity component resulting in a simple circular vortex and induced advective behavior with clockwise circulation in the direction of the flow stream. Because of this vortex, the interfacial area between the two liquids is greatly increased and the mixing has progressed through the channel. However, the mixing of the two water inlets injected in experiments would not make a significant different mixing behavior compared to the analyses for water and methyl alcohol injected through each channel inlet. Mixing due to advective flow generated by the slanted mixer was much more effective than the purely diffusive mass transfer between liquid mixtures [1]. Therefore numerical and experimental results would be in good agreement as shown in Fig. 4.

3.2. Parametric study: effect of design variables

Formulating a full quadratic equation for the response surface using functional variables requires verifying the form of each functional variable and determining whether the objective function is expressed in the form of a second-order parabolic curve. In Fig. 5, we can show the relationship between the design variable and the objective function ΔL_{95} within design domain while restricting

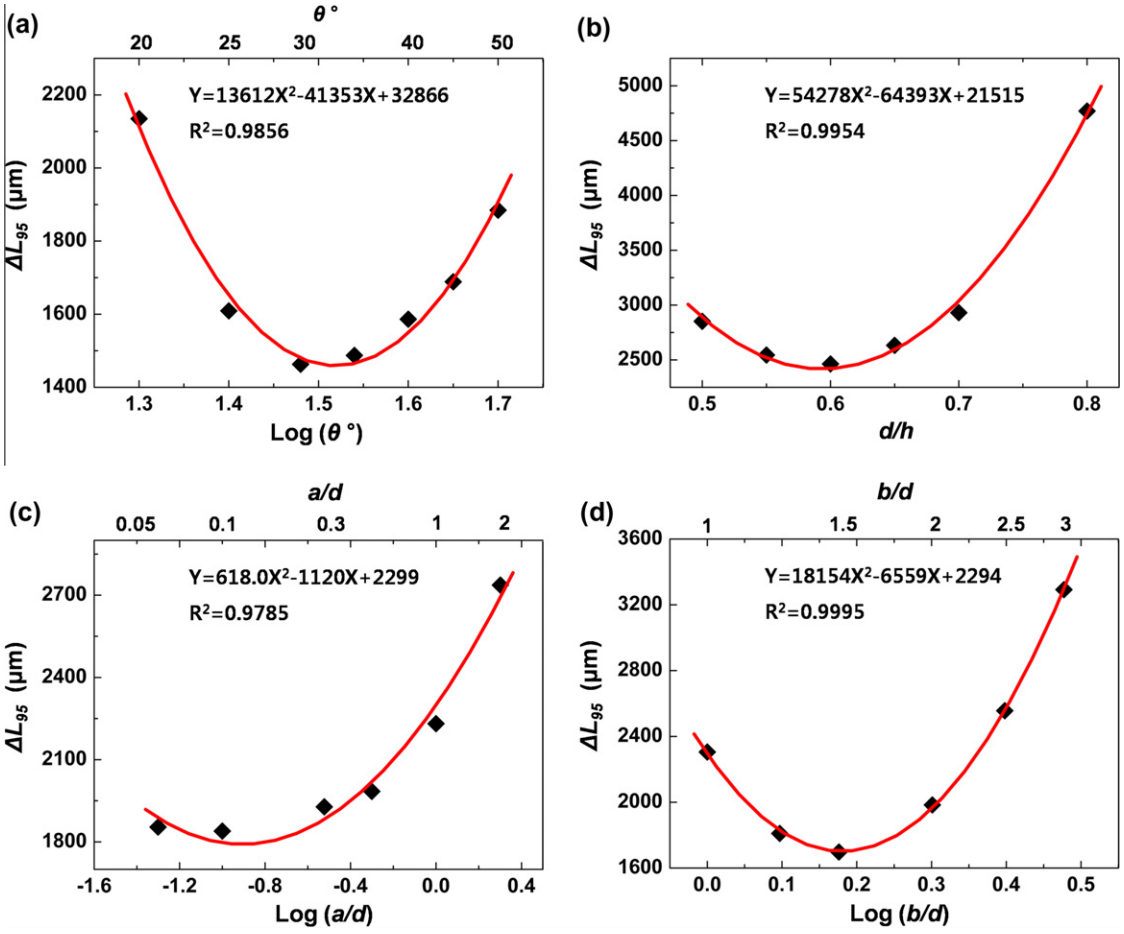

Fig. 5. Objective function ΔL_{95} for each design variable with second-order characteristic curves: (a) effect of θ at $d/h = 0.65$, $a/d = 0.4$ and $b/d = 1.2$, (b) effect of d/h at $\theta = 30°$, $a/d = 1.5$ and $b/d = 2$, (c) effect of a/d at $\theta = 30°$, $d/h = 0.6$ and $b/d = 2$, and (d) effect of b/d at $\theta = 30°$, $d/h = 0.6$ and $a/d = 0.5$.

the other design variables to constant values. From these, we can determine how each design variable affects the mixing characteristics, i.e., the channel length required to obtain adequate mixing performance. In particular, Fig. 5a depicts the objective function ΔL_{95} as a function of the logarithm of the rib angle; the values lie close to a second-order polynomial curve. The fitted equations and the R^2 values for describing the asymptotic curve are shown. Fig. 5c and d also shows the characteristic curves for the functional variables of the logarithm of a/d and the logarithm of b/d, respectively. Fig. 5b shows the characteristic curve for the original d/h expressed directly as a second-order polynomial equation without a functional variable. Therefore, in this study, we make use of functional variables, $log(x_1)$, $log(x_3)$, and $log(x_4)$ as well as the original form x_2 for the full quadratic equation for the response surface.

3.3. Micromixer optimization and design correlations

We can present the surface response functions with the coefficients of Table 2 as a function of four design variables. Table 2 presents the coefficients of a response surface equation estimated from the processes. These numeric results are not indicators that explain the physical phenomena of mixing characteristics with design variables, but just terms that reflect the optimal value and correlations in the restricted range of design variables [22,34]. The magnitude of coefficients except for a constant indicates the intensity of the influence by each term on the objective function. From such results, we can predict that d/h and θ will be more dominant than the others.

Based on these response surfaces, the channel with mixers was optimized when the slanted rib angle was 35.6° with $d/h = 0.7$, $a/d = 0.127$, and $b/d = 1.10$. The optimal geometry for the width of the rib and spacing between ribs was similar to that observed in previous research though the geometrical boundary condition and design variables were not exactly the same [16,17,22]. The optimized rib-shape mixer was much thinner than the spacing between ribs. However, as an additional geometrical design variable, the angle of mixer could affect the mixing performance related to the channel aspect ratio. In contrary, we obtained a different result for slant angle than what has been reported in previous studies with different value of channel aspect ratio. Previous researchers analytically derived the result showing that the maximum transverse flow was achieved at $\theta = 45°$ when the channel aspect ratio was not unity ($w \gg h$) [1,17]. Lynn and Dandy [22] reported that maximum mixing performance was obtained at the channel aspect ratio, w/h of 3.333 with the fixed angle of 45°. Thus their optimized results for the slanted rib angle of the mixer were different from our own cases, which had a channel aspect ratio of unity, as shown in Fig. 1.

The streamlines of the liquids and the series of concentration contours clearly illustrate the helical-shaped advective motion in the direction of the flow stream and the mixing behavior. Here we presented the streamline, mass fraction contour of methyl alcohol, and the velocity vector of each cross-section located in front of the optimized mixers (Fig. 6). The streams started to rotate due to the transverse velocity component induced by the slanted mixers, and enlarged the interfacial area between the liquids. Here, the minimum value of ΔL_{95} estimated by the RSM approximation was 1344 μm, which is between the 14th and 15th mixers. Such a value deviates from the calculated results for the optimal mixer structure by only about 4.41%. Fig. 7 presents the distribution of the percentage mixed, $P(\%)$ along the flow streams for the optimal and three reference models. We can demonstrate that the mixture uniformity increases along the flow direction through the microchannel and is highly affected by the mixer geometries. For the optimal case, the required channel length is 32.3% shorter than that of the aforementioned reference model (ref_1 in Fig. 7) that was used for comparison between analysis and experiments with θ, d/h, a/d, and b/d of 30°, 0.6, 0.5, and 2, respectively.

Table 2
Coefficients for the full quadratic equation using RSM.

Term	Coefficient	Term	Coefficient	Term	Coefficient
Const.	64525	$log(x_1)$	−48528	x_2	−69881
$log(x_3)$	−617.10	$log(x_4)$	−44940	$log(x_1) \cdot x_2$	−1643.6
$log(x_1) \cdot log(x_3)$	333.50	$log(x_2) \cdot log(x_4)$	10315	$x_2 \cdot log(x_3)$	1187.0
$x_2 \cdot log(x_4)$	40988	$log(x_3) \cdot log(x_4)$	1220.7	$[log(x_1)]^2$	15922
$[log(x_2)]^2$	50394	$[log(x_2)]^2$	590.90	$[log(x_4)]^2$	15907

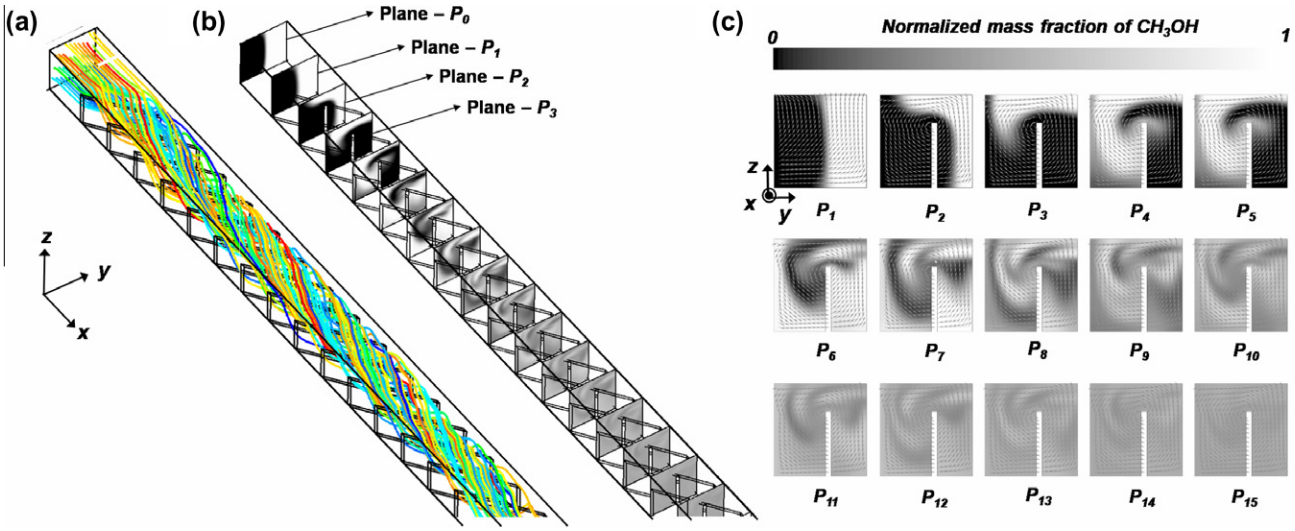

Fig. 6. Numerical analysis results for streamlines and mass fraction contours of CH_3OH in each cross-section when the optimal mixers are installed in the microchannel: (a) streamlines, (b) normalized mass fraction of CH_3OH in the channel, and (c) mass fraction of CH_3OH at the cross-section planes.

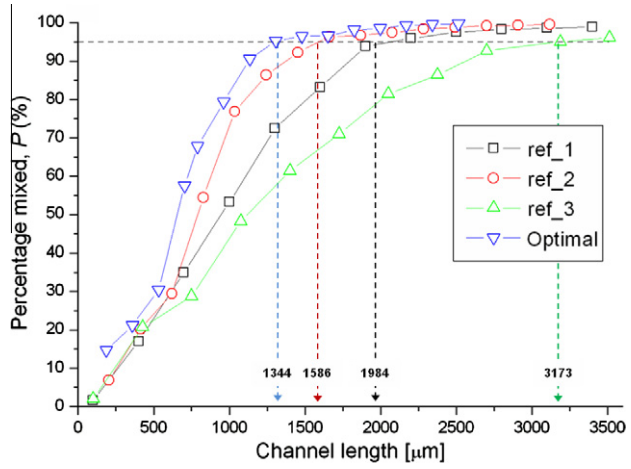

Fig. 7. Comparison of ΔL_{95} for the optimal case and references: for ref_1, $\theta = 30°$, $d/h = 0.6$, $a/d = 0.5$ and $b/d = 2$, for ref_2, $\theta = 40°$, $d/h = 0.65$, $a/d = 0.4$ and $b/d = 1.2$, for ref_3, $\theta = 44.8°$, $d/h = 0.67$, $a/d = 0.148$ and $b/d = 2.29$, respectively.

Fig. 8 shows a two-dimensional contour plot for the resultant maps of objective function ΔL_{95} in the design domain given in Table 1. Fig. 8a shows the design map as a function of θ and d/h for $a/d = 0.127$ and $b/d = 1.10$. Fig. 8b shows the design map as a function of θ and a/d for $d/h = 0.7$ and $b/d = 1.10$, while Fig. 8c shows the design map as a function of θ and b/d for $d/h = 0.7$ and $a/d = 0.127$. As shown in Fig. 8a, ΔL_{95} increased as d/h decreased or as θ recedes from 35.6°. The liquid flow accelerated when d/h increased because the cross-sectional area between the top of the mixer and the channel wall decreased. This brought about an increase in the transverse component of the velocity for the circular vortex, and thus ΔL_{95} decreased. Fig. 8b and c shows that ΔL_{95} increased when a/d decreased below about 0.218 and b/d increased above 1.097, respectively. In both cases, optimal performance occurred at θ of up to 36.0°.

Especially, to make a guideline for practical designs of micromixer with design limitations, optimal design lines that indicate the value of d/h and a/d with the minimum channel length at 95% of mixing performance can be described as a function of θ. These evaluated guidelines present the combined effects of two design variables in each design domain when the others are fixed at certain conditions (here, as optimal values). Two guidelines are presented as following equations:

$$(a/d)_{opt} = 1.03502\theta^2 - 74.8026\theta + 1351.64 \quad (8)$$

$$(b/d)_{opt} = 0.0002404\theta^2 - 0.02764\theta + 1.778 \quad (9)$$

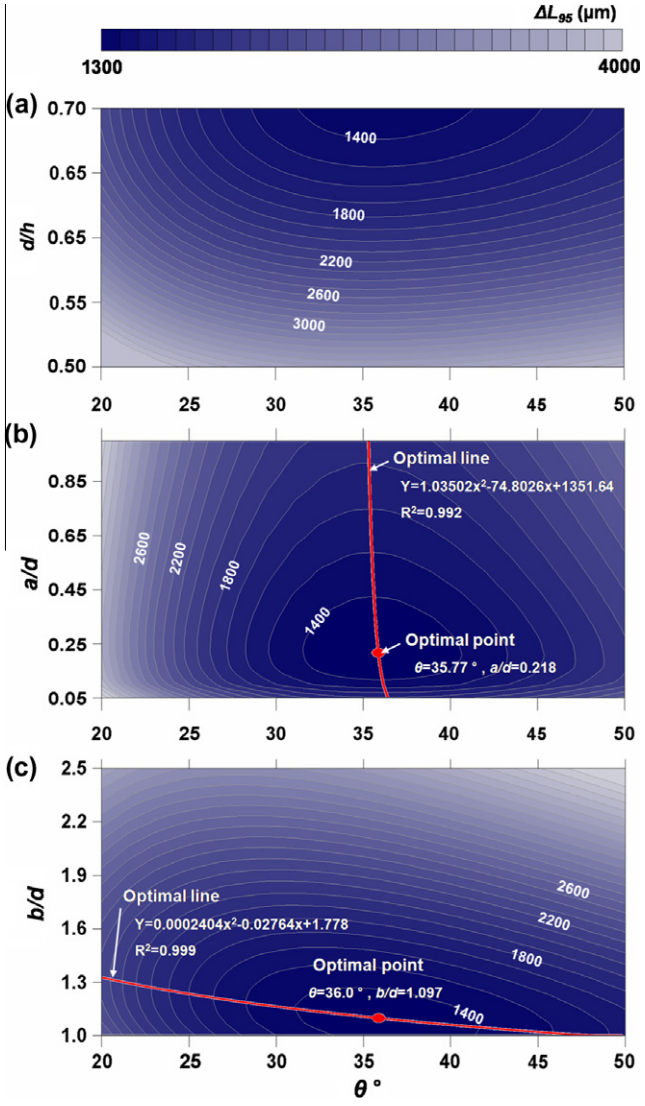

Fig. 8. Resultant maps for ΔL_{95} at various design variables in the design space.

4. Conclusion

On a mass transport performance, we evaluated the optimal design point for a 3D micromixer and correlations as a function of design variables to improve and maximize the mixing performance with uniform mixture concentration. We considered four design variables simultaneously; rib angle, ratio of rib height to channel height, ratio of rib width to rib height, and ratio of rib spacing to rib height. Prior to optimization, we estimate mixing characteristics of the diffusive/convective behavior of liquids by numerical analyses and experiments. We also conducted the parametric studies to evaluate the effect of each design variable on a objective function and determine the form of each functional variable. Using α-RSM with functional variables, we evaluate the optimal design point and correlations as a function of design variable. The optimal value of θ to minimize the channel length was determined to be about 35.6°. The other design variables, d/h, a/d, and b/d, were 0.7, 0.127, and 1.10, respectively. For these mixer geometries, the required channel length that minimized the objective function ΔL_{95} was 1344 μm, which is 32.2% shorter than the reference model with θ, d/h, a/d, and b/d of 30°, 0.6, 0.5, and 2, respectively. Especially for the guideline to practical design of micromixer, optimal design functions were presented as a function of θ. These indicate the value of d/h and a/d with the minimum channel length for uniform mixture concentration.

These results and procedures for the optimization of micromixer can be comprehensively applied to not only design different types of micromixer structures but develop optimal lab-on-a chip devices. For our future work, the optimized mixer from this study would be adapted to the microcalorimeter which detects the heat of reaction between bio-agents like normal human cells and cancer cells [12]. The practical application of α-RSM could improve the sensitivity and reliability of the microfluidic sensing devices by minimizing the lengthscale of devices and optimizing mixing performance.

Acknowledgment

This work was supported by the National Research Foundation of Korea (NRF) grant funded by the Korea government (MEST) (No. 2010-0000504). And this work was also partly supported from Kor-

ea Institute of Environmental Science and Technology (Grant No. 101-082-035). This work was also supported by the Korea Research Foundation Grant funded by the Korean Government (MOEHRD program) (KRF-2008-314-D00143).

References

[1] A.D. Stroock, S.K.W. Dertinger, A. Ajdari, I. Mezic, H.A. Stone, G.M. Whitesides, Chaotic mixer for microchannels, Science 295 (2002) 647–651.
[2] J.M. Ottino, S. Wiggins, Designing optimal micromixers, Science 305 (2004) 485–486.
[3] T. Bayraktar, S.B. Pidugu, Characterization of liquid flows in microfluidic systems, Int. J. Heat Mass Transf. 49 (2006) 815–824.
[4] S.K. Hong, D.H. Lee, H.H. Cho, Heat/mass transfer in rotating impingement/effusion cooling with rib turbulators, Int. J. Heat Mass Transf. 52 (2009) 3109–3117.
[5] K.M. Kim, S.H. Park, Y.H. Jeon, D.H. Lee, H.H. Cho, Heat/mass transfer characteristics in angled ribbed channels with various bleed ratios and rotation numbers, J. Turbomach.-Trans. ASME 130 (2008) 031021.
[6] G.B.N. Boum, S. Martemianov, A. Alemany, Computational study of laminar flow and mass transfer around a surface-mounted obstacle, Int. J. Heat Mass Transf. 42 (1999) 2849–2861.
[7] J.T. Liu, X.F. Peng, W.M. Yan, Numerical study of fluid flow and heat transfer in microchannel cooling passages, Int. J. Heat Mass Transf. 50 (2007) 1855–1864.
[8] M. Meis, F. Varas, A. Velazquez, J.M. Vega, Heat transfer enhancement in microchannels caused by vortex promoters, Int. J. Heat Mass Transf. 53 (2010) 29–40.
[9] W.N. Vreeland, L.E. Locascio, Using bioinspired thermally triggered liposomes for high-efficiency mixing and reagent delivery in microfluidic devices, Anal. Chem. 75 (2003) 6906–6911.
[10] K. Hosokawa, K. Sato, N. Ichikawa, M. Maeda, Power-free poly(dimethylsiloxane) microfluidic devices for gold nanoparticle-based DNA analysis, Lab Chip 4 (2004) 181–185.
[11] J.S. Park, H.I. Jung, Multiorifice flow fractionation: continuous size-based separation of microspheres using a series of contraction/expansion microchannels, Anal. Chem. 81 (2009) 8280–8288.
[12] B.S. Kwak, B.S. Kim, H.H. Cho, J.S. Park, H.I. Jung, Dual thermopile integrated microfluidic calorimeter for biochemical thermodynamics, Microfluid. Nanofluid. 5 (2008) 255–262.
[13] B.S. Kim, B.S. Kwak, S. Shin, H.I. Jung, H.H. Cho, Evaluation of mixing performance and design optimization of a rib-roughened type passive micromixer, in: Joint International Symposia on 3rd Micro & Nanotechnology and Micro/Nanoscale Energy Convergion & Transport-2010, Seoul, Korea, 2010.
[14] K.W. Lin, J.T. Yang, Chaotic mixing of fluids in a planar serpentine channel, Int. J. Heat Mass Transf. 50 (2007) 1269–1277.
[15] A.P. Sudarsan, V.M. Ugaz, Multivortex micromixing, Proc. Natl. Acad. Sci. USA 103 (2006) 7228–7233.
[16] A.D. Stroock, S.K. Dertinger, G.M. Whitesides, A. Ajdari, Patterning flows using grooved surfaces, Anal. Chem. 74 (2002) 5306–5312.
[17] F. Schonfeld, S. Hardt, Simulation of helical flows in microchannels, Aiche J. 50 (2004) 771–778.
[18] D.S. Kim, S.W. Lee, T.H. Kwon, S.S. Lee, A barrier embedded chaotic micromixer, J. Micromech. Microeng. 14 (2004) 798–805.
[19] P.B. Howell, D.R. Mott, S. Fertig, C.R. Kaplan, J.P. Golden, E.S. Oran, F.S. Ligler, A microfluidic mixer with grooves placed on the top and bottom of the channel, Lab Chip 5 (2005) 524–530.
[20] H.Z. Wang, P. Iovenitti, E. Harvey, S. Masood, Numerical investigation of mixing in microchannels with patterned grooves, J. Micromech. Microeng. 13 (2003) 801–808.
[21] D.G. Hassell, W.B. Zimmerman, Investigation of the convective motion through a staggered herringbone micromixer at low Reynolds number flow, Chem. Eng. Sci. 61 (2006) 2977–2985.
[22] N.S. Lynn, D.S. Dandy, Geometrical optimization of helical flow in grooved micromixers, Lab Chip 7 (2007) 580–587.
[23] K.M. Kim, H. Lee, B.S. Kim, S. Shin, D.H. Lee, H.H. Cho, Optimal design of angled rib turbulators in a cooling channel, Heat Mass Transf. 45 (2009) 1617–1625.
[24] A. Bertsch, S. Heimgartner, P. Cousseau, P. Renaud, Static micromixers based on large-scale industrial mixer geometry, Lab Chip 1 (2001) 56–60.
[25] Q. Mei, Z. Xia, F. Xu, S.A. Soper, Z.H. Fan, Fabrication of microfluidic reactors and mixing studies for luciferase detection, Anal. Chem. 80 (2008) 6045–6050.
[26] B.S. Kim, B.S. Kwak, S. Shin, H.I. Jung, H.H. Cho, Diffusive behavior of liquids in microfluidic channel with rib-shape passive micro mixer, in: Proceedings of the 7th JSME-KSME Thermal and Fluids Engineering Conference, Sapporo, Japan, 2008.
[27] T.J. Johnson, D. Ross, L.E. Locascio, Rapid microfluidic mixing, Anal. Chem. 74 (2002) 45–51.
[28] J.M. Ottino, The Kinematics of Mixing: Stretching, Chaos, and Transport, Cambridge University Press, Cambridge, 1989.
[29] W.M. Kays, M.E. Crawford, B. Weigand, Convective Heat and Mass Transfer, McGraw-Hill Higher Education, Boston, 2005.
[30] A.F. Mills, Basic Heat and Mass Transfer, Prentice Hall, Upper Saddler River, NJ, 1999.
[31] J.C. Tannehill, D.A. Anderson, R.H. Pletcher, Computational Fluid Mechanics and Heat Transfer, Taylor & Francis, Washington, DC, 1997.
[32] ANSYS, Fluent 6.3 User's Guide, 2006.
[33] M.A. Ansari, K.Y. Kim, Shape optimization of a micromixer with staggered herringbone groove, Chem. Eng. Sci. 62 (2007) 6687–6695.
[34] R.H. Myers, D.C. Montgomery, Response Surface Methodology: Process and Product Optimization Using Designed Experiments, Wiley, New York, 2002.
[35] M.S. Kim, K.S. Lee, S. Song, Effects of pass arrangement and optimization of design parameters on the thermal performance of a multi-pass heat exchanger, Int. J. Heat Fluid Flow 29 (2008) 352–363.
[36] K.M. Kim, B.S. Kim, D.H. Lee, H. Moon, H.H. Cho, Optimal design of transverse ribs in tubes for thermal performance enhancement, Energy 35 (2010) 2400–2406.
[37] T.J. Mitchell, An algorithm for the construction of "D-optimal" experimental designs, Technometrics 42 (2000) 48–54.